

MOL #80184

**Fe<sup>2+</sup> block and permeation in Ca<sub>v</sub>3.1 (α1G) T-type calcium channels.  
A candidate mechanism for non-transferrin-mediated Fe<sup>2+</sup> influx**

Kyle V. Lopin, I. Patrick Gray, Carlos A. Obejero-Paz, Frank Thévenod, and  
Stephen W. Jones

Department of Physiology and Biophysics, Case Western Reserve University,  
Cleveland, OH 44106, USA (K.V.L., I.P.G., C.A.O., S.W.J.); Universität  
Witten/Herdecke, ZBAF, Institut für Physiologie & Pathophysiologie, Witten,  
Germany (F.T.).

MOL #80184

Running Title: Fe<sup>2+</sup> block and permeation in Cav3.1T-type calcium channels

Corresponding Author:

Stephen W. Jones

Department of Physiology and Biophysics

Case Western Reserve University

Cleveland, OH 44106, USA

Phone: (216) 368-5527

Fax: (216) 368-5586

e-mail: [swj@case.edu](mailto:swj@case.edu)

33 pages

8 figures

60 references

245 words in Abstract

436 words in Introduction

1281 words in Discussion

Nonstandard abbreviations:

$K_D$	Dissociation constant
$\delta$	Fractional electrical distance (from the extracellular side)
$\sigma$	Surface charge density
$\tau$	Time constant
$P_{O,r}$	Relative $P_O$
ferrozine	3-(2-Pyridyl)-5,6-diphenyl-1,2,4-triazine-4',4''-disulfonic acid

MOL #80184

## ABSTRACT

Iron is a biologically essential metal, but excess iron can cause damage to the cardiovascular and nervous systems. We have examined the effects of  $\text{Fe}^{2+}_o$  on permeation and gating in  $\text{Ca}_v3.1$  channels, stably transfected in HEK 293 cells, using whole-cell recording. Precautions were taken to maintain iron in the  $\text{Fe}^{2+}$  state (e. g., extracellular ascorbate). Using instantaneous I-V relations (measured following strong depolarization) to isolate effects on permeation,  $\text{Fe}^{2+}_o$  rapidly blocked currents with 2 mM  $\text{Ca}^{2+}_o$  in a voltage-dependent manner, described by a Woodhull model with  $K_D = 2.5$  mM at 0 mV and an apparent electrical distance  $\delta = 0.17$ .  $\text{Fe}^{2+}_o$  also shifted activation to more depolarized voltages (by  $\sim 10$  mV at 1.8 mM  $\text{Fe}^{2+}_o$ ), somewhat more strongly than  $\text{Ca}^{2+}_o$  or  $\text{Mg}^{2+}_o$ , consistent with a Gouy-Chapman-Stern model with a surface charge density  $\sigma = 1 e^-/98 \text{ \AA}^2$  and  $K_{\text{Fe}} = 4.5 \text{ M}^{-1}$  for  $\text{Fe}^{2+}_o$ . In the absence of  $\text{Ca}^{2+}_o$  (and with  $\text{Na}^+_o$  replaced by tetraethylammonium),  $\text{Fe}^{2+}$  carried detectable whole-cell inward currents at millimolar concentrations ( $73 \pm 7$  pA at -60 mV with 10 mM  $\text{Fe}^{2+}_o$ ). From a 2-site 3-barrier Eyring model for permeation in  $\text{Ca}_v3.1$ , we estimate a transport rate for  $\text{Fe}^{2+}$  of  $\sim 20$  ions per second per open channel at -60 mV and pH 7.2, in 1  $\mu\text{M}$   $\text{Fe}^{2+}_o$  (with 2 mM  $\text{Ca}^{2+}_o$ ). Since  $\text{Ca}_v3.1$  exhibits a significant ‘window current’ in that voltage range ( $P_O \sim 1\%$ ),  $\text{Ca}_v3.1$  channels are a likely pathway for  $\text{Fe}^{2+}$  entry into cells, at clinically relevant concentrations of  $\text{Fe}^{2+}_o$ .

MOL #80184

## Introduction

Iron enters cells not only via the well-characterized transferrin receptor-endocytosis pathway for ferric iron, but also the ill-defined non-transferrin bound iron (NTBI) mechanism for both ferric and ferrous iron entry (Anderson and Vulpe, 2009). Candidate mechanisms for NTBI include the divalent metal-ion transporter DMT1, Zip14 (Liuzzi et al., 2006), the non-selective TRPC6 channel (Mwanjewe and Grover, 2004), and voltage gated calcium channels. Both L-type (Oudit et al., 2003; Tsushima et al., 1999) and T-type (Kumfu et al., 2011) calcium channels have been implicated in  $\text{Fe}^{2+}$  uptake using selective blockers. Currents carried by  $\text{Fe}^{2+}$  have been recorded electrophysiologically for L-channels (Tsushima et al., 1999) but not T-channels.

Iron overload is typically caused by excess dietary absorption of iron in genetic hemochromatosis (Clark et al., 2010) or repeated blood transfusions when red blood cells are broken down and the heme-bound iron is released (Kwiatkowski, 2011). Plasma NTBI can reach  $\sim 5 \mu\text{M}$  (Loreal et al., 2000). NTBI is highly reactive and can cause the formation of damaging free radicals. Excess iron accumulates mainly in the liver and the heart (Andrews, 1999). In myocardial cells, iron overload affects cellular structure (Iancu et al., 1987), gene expression (Parkes et al., 2000),  $\text{Ca}^{2+}$  handling (Kim et al., 1995), and ion channel properties (Kuryshv et al., 1999). Because  $\text{Ca}_v3.1$  channels are widely expressed in excitable and nonexcitable cells including brain, ovary, placenta, heart, liver and vascular smooth muscle (Perez-Reyes, 2003; Rodman et al., 2005; Yunker and McEnery, 2003) understanding the mechanism of  $\text{Fe}^{2+}$  transport by these channels is necessary to understand their role in organ damage in conditions associated with iron overload.

Besides a role as pore blocker and permeant ion (Tsushima et al., 1999; Winegar et al., 1991),  $\text{Fe}^{2+}$  might have significant effects on channel gating as is the case for other divalent cations (Elinder and Arhem, 2003). Gating changes induced by divalent cations

MOL #80184

may rise from pore occupancy, allosteric effects of binding to sites outside the pore (Beedle et al., 2002; Kang et al., 2005; Traboulsie et al., 2007), or by screening or binding to surface charge (Zhou and Jones, 1995).

We find that  $\text{Fe}^{2+}$  blocks currents carried by  $\text{Ca}^{2+}$  or  $\text{Ba}^{2+}$  by voltage-dependent block within the pore.  $\text{Fe}^{2+}$  also permeates, less well than  $\text{Ca}^{2+}$  or  $\text{Ba}^{2+}$ . Effects of  $\text{Fe}^{2+}$  on gating are consistent with a surface charge mechanism, where  $\text{Fe}^{2+}$  both screens and binds to surface charge. The effects of  $\text{Fe}^{2+}$  to block and shift gating would be minimal at clinically observed concentrations of  $\text{Fe}^{2+}$ . However, the estimated rates of  $\text{Fe}^{2+}$  permeation suggest that  $\text{Cav}3.1$  may be a significant source of  $\text{Fe}^{2+}$  entry into cells even at the resting potential.

MOL #80184

## Materials and Methods

**Electrophysiology.** Patch clamp experiments were performed in the whole-cell configuration using HEK 293 cells stably transfected with Ca<sub>v</sub>3.1 (α1G) calcium channels, as described (Khan et al., 2008). Electrodes were made from borosilicate glass, with open pipet resistances of 1.8-2.3 MΩ, and access resistances of 5 ± 1 MΩ before compensation (80%). Currents were digitally sampled at 50 kHz after 10 kHz analog filtering using an Axopatch 200 amplifier and pClamp 8.2 software. Leak and capacitive currents were subtracted online using a P/-4 protocol. Experiments were performed at room temperature (~22 °C).

We evaluated the effect of Fe<sup>2+</sup> using two basic voltage protocols, IV (direct depolarization to a range of voltages) and IIV (preactivating channels by strong, brief depolarization, followed by steps to a range of voltages) (Figs. 1-2). Assuming effects of Fe<sup>2+</sup> are effectively instantaneous (as we conclude below), this approach allows separation of effects on permeation vs. gating (Hodgkin and Huxley, 1952; Khan et al., 2008; Lopin et al., 2012; Obejero-Paz et al., 2008; Serrano et al., 1999). Currents measured immediately following repolarization with the IIV protocol (Fig. 1A) should be directly proportional to the current through a single open channel. Thus, effects of Fe<sup>2+</sup> on the IIV relationship should reflect inhibition of current through open channels. Effects on the IV relationship, in contrast, reflect the net effect of the ion both on permeation and on gating.

**Standard recording solutions.** The intracellular solution contained (in mM) 2 CaCl<sub>2</sub>, 1 MgCl<sub>2</sub>, 120 NaCl, 10 HEPES, 4 MgATP, and 11 EGTA, adjusted to pH 7.2 with NaOH (total Na<sup>+</sup> 145 mM, calculated free Ca<sup>2+</sup> 70 nM). The normal extracellular solution contained 2 CaCl<sub>2</sub>, 128 NaCl, 5 ascorbic acid, 10 glucose, 20 HEPES, adjusted to pH 7.2 with NaOH (total Na<sup>+</sup> 145 mM). When noted, CaCl<sub>2</sub> was replaced by BaCl<sub>2</sub>.

MOL #80184

**Extracellular solutions containing Fe<sup>2+</sup>.** Extreme care must be taken to maintain iron in the soluble Fe<sup>2+</sup> state. To do this FeCl<sub>2</sub> was added to the solution only after cells were patched and control currents were being recorded to reduce the amount of time Fe<sup>2+</sup> could oxidize. Solutions were made 1-2 minutes before they were applied to the cells and were used within the 6 minutes of being made. Fe<sup>2+</sup> was added to the final desired concentration from a 200 mM stock solution of FeCl<sub>2</sub>·4 H<sub>2</sub>O in 1% HCl (v/v). Each solution was measured for free Fe<sup>2+</sup> using the ferrozine method (Dorey et al., 1993; Viollier et al., 2000) while the electrophysiological experiments were being performed. To this end a sample of the extracellular solution was diluted to a final concentration of 100 μM Fe<sup>2+</sup> with a solution containing the same components (except FeCl<sub>2</sub>), or a solution containing 5 mM ascorbate (pH 3.3) to reduce all iron forms. 0.75 ml of those samples were mixed with the same volume of 2 mM ferrozine, and absorbance was measured (at 562 nm) in a Beckman DU640B spectrophotometer. Standards in the range from 10 μM and 100 μM Fe<sup>2+</sup> were prepared by dilution of a stock solution of 20 mM FeCl<sub>2</sub>·4 H<sub>2</sub>O, with a final concentration of 5 mM ascorbic acid. Measured free Fe<sup>2+</sup> concentrations ranged from 28 – 95% of the nominal value. Throughout this paper, the values for Fe<sup>2+</sup> concentration are the actual values measured by this procedure.

For experiments examining block by Fe<sup>2+</sup>, Fe<sup>2+</sup> was added to the normal extracellular solutions (2 mM Ca<sup>2+</sup> or 2 mM Ba<sup>2+</sup>). To investigate whether Cav3.1 currents allow Fe<sup>2+</sup> influx, we designed extracellular solutions where Fe<sup>2+</sup> was the only charge carrier. To this end extracellular NaCl was replaced by TEA-Cl, Ca<sup>2+</sup> by Fe<sup>2+</sup>, and solutions were maintained at pH 7.0 to reduce the rate of iron oxidation. A pH of 6.8 – 7.05 measured at the end of the experiment was considered acceptable. A control solution containing 2 mM Ca<sup>2+</sup> was applied to the cell before and after the test solution.

Since inward currents were small with Fe<sup>2+</sup>, we performed experiments to evaluate the contribution of gating currents, using an extracellular solution containing (mM) 140 NaCl, 2 CdCl<sub>2</sub>, and 1 mM LaCl<sub>3</sub>.

**Data Analysis.** Most methods were as described (Lopin et al., 2012). Throughout the paper, data are shown as mean  $\pm$  sem. We used the paired t-test implemented in Origin 7.0 (OriginLab corporation) to assess differences between means when controls were from the same cell. We used one way ANOVA to investigate differences between means from different groups. A two tailed  $p < 0.05$  was considered statistically significant.

**Fe<sup>2+</sup> block.** The voltage dependence of block by Fe<sup>2+</sup> was described by a model that assumes that Fe<sup>2+</sup> binds within the electrical field of the membrane, with Fe<sup>2+</sup> entry and exit exclusively from the extracellular solution (Woodhull, 1973)

$$f = 1 / \left\{ 1 + [Fe^{2+}] / \left( K_{D,0} e^{\frac{z\delta FV}{RT}} \right) \right\} \quad (1)$$

where  $f$  is the fraction of peak tail current remaining in the presence of Fe<sup>2+</sup>, and  $K_{D,0}$  is the  $K_D$  at 0 mV.

**Permeation model.** The classical 2-site 3-barrier model of channel permeation (2S3B) (Almers and McCleskey, 1984; Hess and Tsien, 1984), was extended to Fe<sup>2+</sup>, as for Cd<sup>2+</sup> (Lopin et al., 2010; Lopin et al., 2012). In brief, parameters for the energy profile of Fe<sup>2+</sup> were chosen that minimized the sum of absolute error to currents recorded due to Fe<sup>2+</sup> block and permeation. The parameters for Ca<sup>2+</sup>, Ba<sup>2+</sup>, Mg<sup>2+</sup>, and Na<sup>+</sup> were fixed to the parameters from Lopin et al. (2010) where they were fit to a wide range of ionic conditions. The minimization procedure produced multiple parameters sets with similar errors (within 15%), all with qualitatively similar currents and energy profiles (all energy parameters varied in a 1 kT range across parameter sets). Because we use the model to predict Fe<sup>2+</sup> transport rates we chose the parameter set that best fit the currents carried by Fe<sup>2+</sup>. All other parameter sets predicted Fe<sup>2+</sup> currents larger than were observed. They also predicted Fe<sup>2+</sup> transport rates up to twice as large as the parameter set chosen in this paper.

MOL #80184

Because control currents in  $\text{Fe}^{2+}$  permeation experiments were significantly larger than controls in experiments from Khan et al. (2008), we assumed 18000 channels per cell as opposed to 8000. We expect that  $\text{Fe}^{2+}$  currents are minimally affected by the 0.2 pH unit difference between solutions. Because it was not always possible to record control currents after the test solution we used the first control for normalization, a procedure that will underestimate the iron currents in the presence of current run-down.

**Gating.** To investigate the effect of  $\text{Fe}^{2+}$  on channel activation we fitted simultaneously relative open probability ( $P_{O,R}$ ) measured in controls and  $\text{Fe}^{2+}$  to a fourth-power Boltzmann function

$$P_{O,R}(V) = \left( \frac{1}{1 + e^{\left( \frac{-(V - (V_{0.5} - \delta \Delta V_{0.5}))}{k} \right)}} \right)^4 \quad (2)$$

where  $V_{0.5}$  is the half point of activation of each individual voltage sensor,  $k$  is the voltage sensitivity, and  $\Delta V_{0.5}$  is the shift in  $V_{0.5}$  induced by  $\text{Fe}^{2+}$  and  $\delta$  is the Kronecker deltafunction where it takes the value of 1 for  $\text{Fe}^{2+}$  and 0 for controls.

The effect of  $\text{Fe}^{2+}$  on the rate of channel opening was addressed indirectly studying changes in the time to peak (TP). To this end we simultaneously fitted data from controls and  $\text{Fe}^{2+}$  to equation 4

$$TP(V) = e^{\left( \frac{-(V - (V_{1-TP\infty} - \alpha \Delta V_{1-TP\infty}))}{k} \right)} + TP_{\infty} \quad (3)$$

where  $V_{1-TP\infty}$  is the voltage at which the time to peak is equal to one minus the asymptotic value of TP ( $TP_{\infty}$ ),  $k$  is the voltage sensitivity and  $\Delta V_{1-TP\infty}$  is the shift along the voltage axis.

The effect of  $\text{Fe}^{2+}$  on the closing rate was investigated fitting simultaneously deactivating time constants between -70 and -120 mV to equation 4

MOL #80184

$$\tau(V) = e^{\left( \ln(2) + \frac{(V - (V_{\tau 2ms} - a \cdot \Delta V_{\tau 2ms}))}{k} \right)} \quad (4)$$

where  $V_{\tau 2ms}$  is the voltage where the time constant equals 2 ms.  $\Delta V_{\tau 2ms}$  is the displacement induced by  $\text{Fe}^{2+}$  along the voltage axis, and  $k$  is the slope factor.

Gating shifts were calculated using the Minerror procedure (Mathcad) to calculate the values of  $\sigma_i$  and  $K_{Fe}$  that minimize  $\chi^2$  for  $\Delta V_{0.5}$ ,  $\Delta V_{1-TP\alpha}$ , and  $\Delta V_{\tau 2ms}$ .

**$^{59}\text{Fe}^{2+}$  kinetic transport studies.** For cellular  $^{59}\text{Fe}^{2+}$  uptake,  $^{59}\text{Fe}^{2+}$  was generated from  $^{59}\text{FeCl}_3$  (specific activity  $>5\text{Ci}(185\text{GBq})/\text{g FeCl}_3$  in 0.5M HCl; Perkin-Elmer, Rodgau, Germany) as described elsewhere (Garrick et al., 2006).  $^{59}\text{Fe}^{2+}$  uptake (18.5 kBq/ml  $^{59}\text{FeCl}_2$  in 200-400  $\mu\text{M FeSO}_4$ ) was performed in confluent monolayers of HEK293 cells or HEK293-Cav3.1, with or without 25  $\mu\text{M}$  NNC 55-0396, a selective inhibitor of T-type calcium channels (Huang et al., 2004). Monolayers were washed with 2 mM desferrioxamine mesylate, solubilized in 1 N NaOH and cellular radioactivity was measured in a  $\gamma$ -counter.

## Results

**Effects of Fe<sup>2+</sup> on permeation.** Extracellular application of Fe<sup>2+</sup> reversibly inhibited currents through Ca<sub>v</sub>3.1 channels evaluated using the IIV protocol (Fig. 1A). In these ionic conditions (2 mM Ca<sup>2+</sup><sub>o</sub> and 145 mM Na<sup>+</sup><sub>i,o</sub>), Ca<sub>v</sub>3.1 channels exhibited inward currents carried mostly by Ca<sup>2+</sup> and outward currents carried by Na<sup>+</sup>. Note that the inward tail currents in Fe<sup>2+</sup> were smaller and faster. Peak tail currents were reduced immediately after repolarization, suggesting that Fe<sup>2+</sup> reached steady-state block rapidly. Block was concentration- and voltage-dependent, with strong inhibition at negative voltages, but little effect on outward currents (Fig. 1B). Fe<sup>2+</sup> had no clear effect on the reversal potential (Fig. 1C). The voltage dependence of block is best illustrated by chord conductances, especially around the reversal potential (Fig. 1D). The fractional inhibition, measured from chord conductances, was well described by a Woodhull (1973) model (Fig. 1E), suggesting negligible relief of block by hyperpolarization. The data were fitted best with K<sub>D</sub> = 2.5 mM at 0 mV, and electrical distance  $\delta = 0.17$ .

**Effects of Fe<sup>2+</sup> on gating.** Fe<sup>2+</sup> also inhibited currents examined with the IV protocol, evoking currents by direct depolarizations from the holding potential (Fig. 2A). The peak current at each voltage is shown in Fig. 2B, on an expanded scale in Fig. 2C, and as chord conductances in Fig. 2D. With this protocol, inhibition by Fe<sup>2+</sup> was also voltage-dependent, stronger at more negative voltages, and the voltage producing peak inward current was shifted to more positive voltages (Fig. 2C). Inhibition of peak current could also be described by a Woodhull (1973) model, with K<sub>D</sub> = 1.4 mM at 0 mV and  $\delta = 0.33$ .

Why does the effect of Fe<sup>2+</sup> appear to be more potent and more voltage-dependent with the IV protocol? The currents recorded in that manner are affected not only by permeation (e. g., channel block), but also by gating (e. g., surface charge effects of Fe<sup>2+</sup>).

MOL #80184

We examined the effects of  $\text{Fe}^{2+}$  on activation by three measures: effects on the time course of channel activation (Fig. 3A) and deactivation (Fig. 3B), and on the voltage-dependence of peak activation (Fig. 3C). Activation curves were measured as the relative open probability ( $P_{O,r}$ ), calculated as the ratio of peak current from the IV protocol divided by the current at that same voltage from the IIV protocol (Fig. 3C) (Khan et al., 2008; Serrano et al., 1999). This is a more accurate reflection of channel open probability than the more commonly used chord conductance, since the open channel conductance is not constant with voltage (Fig. 1D), so the chord conductances measured with the IV protocol (Fig. 2D) are not pure measures of channel activation (Khan et al., 2008). All three measures of the voltage-dependence of channel gating were affected by  $\text{Fe}^{2+}$  in a similar manner (Fig. 3D), demonstrating positive shifts along the voltage axis with  $\text{Fe}^{2+}$ . It is noteworthy that  $\text{Fe}^{2+}$  did not affect the limiting rates for channel activation (Fig. 3A) or inactivation (Fig. 3B) at strongly depolarized voltages.

Qualitatively, the observed voltage shifts were as expected from a surface charge mechanism, where cations screen a negative surface charge on the extracellular side. Quantitatively, the effect was approximately twice as large as previously observed for  $\text{Ca}^{2+}$ ,  $\text{Ba}^{2+}$ , and  $\text{Mg}^{2+}$  (Khan et al., 2008; dashed curve in Fig. 3D). Since simple charge screening (Gouy-Chapman theory) assumes all divalent cations are equivalent, we considered the possibility that  $\text{Fe}^{2+}$  can bind to the surface charge, as well as screening it (Gouy-Chapman-Stern theory), as observed for  $\text{Cd}^{2+}$  (Lopin et al., 2012). Fig. 3D demonstrates that the data can be described well by the same surface charge density previously determined for effects of  $\text{Ca}^{2+}$ ,  $\text{Ba}^{2+}$ , and  $\text{Mg}^{2+}$  ( $\sigma = 1 \text{ e}^-/98 \text{ \AA}^2$ , Khan et al. 2008), but allowing binding of  $\text{Fe}^{2+}$  to the surface charge with  $K_{\text{Fe}} = 4.5 \text{ M}^{-1}$ .

**Effects of  $\text{Fe}^{2+}$  with 2 mM  $\text{Ba}^{2+}$ .**  $\text{Ca}_v3.1$  calcium channels are selective for  $\text{Ca}^{2+}$  over  $\text{Ba}^{2+}$  by the classical criterion of permeability ratios, reflecting a more positive reversal potential with  $\text{Ca}^{2+}$ , indicating greater selectivity vs. monovalent cations (Serrano et al., 2000). Correspondingly, di- and trivalent cations block more rapidly

MOL #80184

and/or strongly when  $\text{Ba}^{2+}$  is the charge carrier, reflecting stronger competition vs. the less permeant  $\text{Ba}^{2+}$  ion ( $\text{Mg}^{2+}$ , Serrano et al., 2000;  $\text{Ni}^{2+}$ , Obejero-Paz et al., 2008;  $\text{Y}^{3+}$ , Obejero-Paz et al., 2005;  $\text{Cd}^{2+}$ , Lopin et al. 2012). That was also observed for  $\text{Fe}^{2+}$  (Figs. 4-5). 0.13 mM  $\text{Fe}^{2+}$  blocked strongly at hyperpolarized voltages, using either the IIV (Figs. 4A, 5A) or IV protocols (Figs. 4B, 5C). Inhibition measured from chord conductances, using the IIV protocol, was described by a Woodhull model with  $K_D = 0.33$  mM at 0 mV and  $\delta = 0.21$  (Fig. 5B). Block was slightly overestimated by the model at the most negative voltages, suggesting relief of block by exit of  $\text{Fe}^{2+}$  into the cell. That low concentration of  $\text{Fe}^{2+}$  had minimal effect on channel activation (Fig. 5D). The activation curve was shifted by  $+2.8 \pm 1.0$  mV, and time constants for activation and deactivation by  $2.9 \pm 0.5$  mV and  $-1.0 \pm 1.6$  mV respectively.

**Permeation by  $\text{Fe}^{2+}$ .** When extracellular  $\text{Ca}^{2+}$  and  $\text{Na}^+$  were replaced by  $\text{Fe}^{2+}$  and TEA (respectively), inward currents were small but clearly detectable (Fig. 6). Currents were larger in 9 mM vs. 1 mM  $\text{Fe}^{2+}$  (Fig. 6C), as expected for permeation by  $\text{Fe}^{2+}$ . The chord conductance in 9 mM  $\text{Fe}^{2+}$  was  $1.5 \pm 0.2$  -fold larger than in 1 mM  $\text{Fe}^{2+}$ , averaged from -150 to -50 mV ( $p < 0.01$ ).

An alternative interpretation is that the inward currents observed in  $\text{Fe}^{2+}$  might be ‘off’ gating currents. To evaluate that possibility, we compared the integrated tail current amplitudes to gating currents, isolated using a combination of 0.1 mM  $\text{La}^{3+}_o$  and 2 mM  $\text{Cd}^{2+}_o$  to block ionic currents (Fig. 7). The insets in Fig. 7A show that the inward currents were larger in  $\text{Fe}^{2+}_o$ . Quantitatively, the integrated  $\text{Fe}^{2+}$  tail current greatly exceeded the gating currents at voltages where tail currents were relatively large and slowly decaying (Fig. 7B). The amplitude of the integrated tail current increased with  $[\text{Fe}^{2+}]_o$  (Fig. 7C). There was considerable scatter in the data, presumably reflecting cell-cell variation in channel expression levels, so the apparent  $K_D$  of 4.7 mM for saturation of current with  $\text{Fe}^{2+}_o$  should be considered a rough estimate.

MOL #80184

Reversal potentials were less positive in  $\text{Fe}^{2+}$  than in  $\text{Ca}^{2+}$  (Fig. 6C),  $-26.1 \pm 4.7$  mV ( $n=4$ ) in 1.1 mM  $\text{Fe}^{2+}$ , and  $-9.0 \pm 3.7$  mV ( $n=5$ ) in 8.9 mM  $\text{Fe}^{2+}$ . Those values correspond to permeability ratios  $P_{\text{Fe}}/P_{\text{Na}} = 16$  or 5, respectively. That compares to  $P_{\text{Ca}}/P_{\text{Na}} = 87$  and  $P_{\text{Ba}}/P_{\text{Na}} = 44$  (Khan et al., 2008), and imply  $P_{\text{Fe}}/P_{\text{Ca}} = 0.06-0.18$ .

Incubation studies with  $^{59}\text{Fe}^{2+}$  were performed and showed a trend towards increased  $\text{Fe}^{2+}$  uptake by  $\text{Ca}_v 3.1$  channels but were inconclusive due to large background uptake of  $\text{Fe}^{2+}$  and increased cell death (data not shown).

**Model for  $\text{Fe}^{2+}$  permeation and block.** We fitted the data on  $\text{Fe}^{2+}$  permeation and block to a 2-site 3-barrier (2S3B) Eyring rate theory model (Almers and McCleskey, 1984). The fit of the model to the data is shown for  $\text{Fe}^{2+}$  permeation (Fig. 8B), and for block of current carried by  $\text{Ca}^{2+}_o$  (Fig. 8C) or  $\text{Ba}^{2+}_o$  (Fig. 8D).

We used the model to estimate the extent of  $\text{Fe}^{2+}$  permeation at concentrations more relevant to physiological or pathophysiological conditions (Fig. 8E-F). Simulated addition of 1-10  $\mu\text{M}$   $\text{Fe}^{2+}$  (to extracellular solutions also containing 2 mM  $\text{Ca}^{2+}_o$ ) yielded predicted  $\text{Fe}^{2+}$  influx at rates up to several hundred ions per second through a single open channel (Fig. 8E). The mechanism of  $\text{Fe}^{2+}$  permeation predicted by the model is similar to the permeation of  $\text{Ca}^{2+}$ , with quantitative differences. Both ions seem to get into the pore and bind to the first site similarly but  $\text{Fe}^{2+}$  is slower to move over to the second site, binds less tightly to second site, and the energy barrier to  $\text{Fe}^{2+}$  exit from the pore is higher.

$\text{Ca}_v3.1$  channels inactivate rapidly and strongly, but inactivation is incomplete, with 1-2% of channels remaining open even after 0.3 sec,  $20\times$  the time constant for inactivation (Serrano et al., 1999). This produces a ‘window current’ that can potentially allow maintained entry of divalent cations into the cell even near the resting potential. When the 2S3B model for permeation was combined with the Serrano et al. (1999) model for gating of  $\text{Ca}_v3.1$ , the predicted steady-state  $\text{Fe}^{2+}$  influx peaked at 6 ions/sec near -60

MOL #80184

mV, in 10  $\mu\text{M}$   $\text{Fe}^{2+}$  (Fig. 8F). Correction for slow inactivation would lower these values by ~35% (Hering et al., 2004).

MOL #80184

## Discussion

We conclude that  $\text{Fe}^{2+}$  affects currents through  $\text{Ca}_v3.1$  channels by three mechanisms: block of the open pore by  $\text{Fe}^{2+}$ , shifts in channel activation, and permeation by  $\text{Fe}^{2+}$ .  $\text{Fe}^{2+}$  permeates  $\text{Ca}_v3.1$  pores poorly, compared to  $\text{Ca}^{2+}$  or  $\text{Ba}^{2+}$  or even  $\text{Cd}^{2+}$  (Lopin et al., 2012), but the estimated rate of  $\text{Fe}^{2+}$  entry suggests that  $\text{Ca}_v3.1$  is a strong candidate for  $\text{Fe}^{2+}$  influx in conditions where free  $\text{Fe}^{2+}_o$  is present at micromolar concentrations. We discuss first the biophysical mechanisms of  $\text{Fe}^{2+}$  interaction with calcium channels, and then the potential implications for iron overload.

**Block by  $\text{Fe}^{2+}$ .** The effect of  $\text{Fe}^{2+}$  on the IIV relationship is consistent with block by occupancy of the pore, presumably at the ‘selectivity filter’ responsible for selectivity for  $\text{Ca}^{2+}$  and other di- and trivalent cations. First, block is voltage-dependent, well approximated by a Woodhull (1973) model assuming binding to a site within the electrical field of the membrane. Second, block was ~4-fold stronger when 2 mM  $\text{Ba}^{2+}$  was the charge carrier (compared to 2 mM  $\text{Ca}^{2+}$ ), suggesting ion-ion competition within the pore. Reduction of the current measured ‘instantaneously’ implies that  $\text{Fe}^{2+}$  equilibrates rapidly with the open pore, on the time scale of the voltage clamp (~0.1 ms). For the lowest concentration used (0.13 mM  $\text{Fe}^{2+}$ , for experiments with  $\text{Ba}^{2+}$ ), that implies binding with a bimolecular rate constant of  $10^8 \text{ M}^{-1}\text{s}^{-1}$  or faster, near the diffusion limit.

**Effects of  $\text{Fe}^{2+}$  on gating.** The effect of  $\text{Fe}^{2+}$  on the peak current measured with the IV protocol was stronger and more voltage-dependent than with the IIV protocol. Since the current measured with the IV protocol is affected both by permeation and gating (i. e., changes in the probability that a channel is open at a particular voltage and time), this suggests that  $\text{Fe}^{2+}$  affects the response of the channel to voltage. Fig. 3 shows that the effect of  $\text{Fe}^{2+}$  can be attributed to screening and binding to surface charge. We

MOL #80184

assumed a Guoy-Chapman-Stern for simplicity but a specific binding site on the channel can not be excluded.

**Fe<sup>2+</sup> permeation.** In the absence of Ca<sup>2+</sup><sub>o</sub> and Na<sup>+</sup><sub>o</sub> Ca<sub>v</sub>3.1 channels carry a significant Fe<sup>2+</sup> current that saturates in the millimolar range. The currents measured in Fe<sup>2+</sup> were small, showing Fe<sup>2+</sup> is a poorly permeant ion, but were noticeable larger than could be attributed to gating charge movement (Fig 7B). This current increased as external Fe<sup>2+</sup> was increased, suggesting that the current is carried by Fe<sup>2+</sup> and not contaminating cations.

**Ca<sub>v</sub>3.1 as a pathway for Fe<sup>2+</sup> entry.** To explain the effects of Fe<sup>2+</sup> on permeation we expanded a model of permeation for Ca<sub>v</sub>3.1 channels to account for Fe<sup>2+</sup>. The model fit the data well, although block of outward currents by 1.1 mM Fe<sup>2+</sup> was underestimated (Fig. 8B). The model can assess Fe<sup>2+</sup> permeation when Ca<sup>2+</sup> and Mg<sup>2+</sup> are present in physiological concentrations. Fig 8E and F show calculated transport rates for Fe<sup>2+</sup> for external concentrations in the range of 1-10 μM and membrane potentials encountered at rest and during action potentials. Ca<sub>v</sub>3.1 channels have a window current due to incomplete inactivation (Serrano et al., 1999) that leaves ~1-2% of channels open at resting membrane potentials. Because channels are open even at resting membrane potentials, we used our model of Ca<sub>v</sub>3.1 channel gating to calculate the fraction of channels expected to be open in the steady state (Serrano et al., 1999). This value, times the transport rate calculated in Fig 8F, is the number of Fe<sup>2+</sup> ions transported per second and channel (Fig 8D).

**Comparison of Fe<sup>2+</sup> to other divalent cations.** We have now examined effects of several divalent cations on permeation and gating of Ca<sub>v</sub>3.1: Ca<sup>2+</sup>, Ba<sup>2+</sup>, Mg<sup>2+</sup>, Ni<sup>2+</sup>, and Cd<sup>2+</sup> (Khan et al., 2008; Lopin et al., 2012; Obejero-Paz et al., 2008). To a surprising extent, each ion is an individual that the channel can easily distinguish. As previously established for L-type calcium channels, there is a spectrum from highly permeant ions to strong blockers. Ca<sup>2+</sup> and Ba<sup>2+</sup> are the most permeant at millimolar concentrations,

MOL #80184

although they also potently block currents carried by  $\text{Na}^+$  at micromolar concentrations.  $\text{Mg}^{2+}$  is nearly impermeant, but blocks currents carried by  $\text{Ca}^{2+}$  from either side of the membrane (Khan et al., 2008).  $\text{Fe}^{2+}$  appears at first to be a  $\text{Mg}^{2+}$ -like blocker, but can carry small inward currents. The classical calcium channel blocker  $\text{Cd}^{2+}$  produces surprisingly large inward currents, and has a reversed voltage-dependence of channel block (Lopin et al., 2012).  $\text{Ni}^{2+}$  seems to be unique in blocking rapidly at an extracellular site (that cannot distinguish  $\text{Ca}^{2+}$  from  $\text{Ba}^{2+}$ ), in addition to slow block at the selectivity filter (Obejero-Paz et al., 2008). Except for the fast block site for  $\text{Ni}^{2+}$ , these effects can be explained by a 2-site 3-barrier model as subtle quantitative changes in the energetics of ion binding, as opposed to distinct biophysical mechanisms.

**Iron overload.** Iron is normally tightly regulated in the body (Zhang and Enns, 2009). Increased intracellular iron has been associated with disorders in both the heart (Horwitz and Rosenthal, 1999; Kremastinos and Farmakis, 2011) and the brain (Stankiewicz and Brass, 2009), including neurological disorders such as amyotrophic lateral sclerosis (ALS), Parkinson's, and Alzheimer's disease (Oshiro et al., 2011). Intracellular iron leads to the production of reactive oxygen species that cause oxidative damage to proteins, lipids, and DNA (Giorgio et al., 2007).

**Pathways for NTBI iron influx.** In neurons, voltage-gated calcium channels (Gaasch et al., 2007) and NMDA receptors (Pelizzoni et al., 2011) have been implicated in NTBI. Studies with calcium channel blockers implicated both L-type channels and non-L high voltage-activated channels in  $\text{Fe}^{2+}$  entry into hippocampal neurons (Pelizzoni et al., 2011). The cerebrospinal fluid has levels of iron that saturate transferrin, leaving  $\sim 1 \mu\text{M}$  free iron (Bradbury, 1997). This iron should be maintained in its ferrous form ( $\text{Fe}^{2+}$ ) by high levels of ascorbate (Bradbury 1999) and ferrireductases (Lane et al., 2010; Mills et al., 2010). In the case of cerebral hemorrhage free iron levels were measured to peak at  $>10 \mu\text{M}$  and to remain above  $5 \mu\text{M}$  for 28 days (Wan et al., 2006). This could provide sufficient free  $\text{Fe}^{2+}$  for entry into neurons via calcium channels.

MOL #80184

The mechanism of  $\text{Fe}^{2+}$  uptake into cardiomyocytes is still debated (Chattipakorn et al., 2011). Block of L-type and T-type calcium channels in cardiomyocytes *in vivo* (Kumfu et al., 2012; Oudit et al., 2003) can decrease iron uptake into the heart, an indication that sufficient free  $\text{Fe}^{2+}$  is available in the plasma for calcium channels, and it can permeate in the presence of physiological levels of  $\text{Ca}^{2+}$ .

While the main mechanism of preventing excess iron in cells is to prevent iron uptake there are mechanisms cells use to efflux excess iron out of the cell, the main protein being ferroportin1 (Fpn1) (Donovan et al., 2000). To maintain iron homeostasis, when iron levels are increased the liver releases hepcidin (Park et al., 2001) which binds to Fpn1 causing its endocytosis and degradation (Nemeth et al., 2004). Normally this reduces plasma iron levels by decreasing Fpn1 in intestinal cells, decreasing iron absorption from the diet (Ganz, 2011). In iron overload conditions where iron absorption is unregulated in this way due to repeated transfusions to treat a blood disorder the mechanism of hepcidin downregulating Fpn1 could cause iron handling problems. In cells with unregulated  $\text{Fe}^{2+}$  entry, such as cardiomyocytes and neurons which have a large number of calcium channels, hepcidin release will cause Fpn1 to decrease (Wang et al., 2010), lowering the capacity of cells to export  $\text{Fe}^{2+}$  while calcium channels continue to allow unregulated  $\text{Fe}^{2+}$  entry.

Our results indicate that  $\text{Ca}_v3.1$  channels can constitute a pathway for iron entry at resting membrane potentials, and possibly during the course of action potentials, when extracellular  $\text{Fe}^{2+}$  reaches concentrations in the micromolar range.

MOL #80184

## Acknowledgements

We thank Dr. Ed Perez-Reyes (U. Virginia) for the HEK 293 cell line stably transfected with Ca<sub>v</sub>3.1.

MOL #80184

## Authorship Contributions

Participated in research design: Lopin, Obejero-Paz, Thévenod, Jones

Conducted experiments: Lopin, Gray, Obejero-Paz, Thevenod

Contributed new reagents or analytical tools: none

Performed data analysis: Lopin, Obejero-Paz, Thévenod, Jones

Wrote or contributed to the writing of the manuscript: Lopin, Obejero-Paz, Thévenod,  
Jones

MOL #80184

## References

- Almers W and McCleskey EW (1984) Non-selective conductance in calcium channels of frog muscle: calcium selectivity in a single-file pore. *J Physiol (Lond)* **353**: 585-608.
- Anderson GJ and Vulpe CD (2009) Mammalian iron transport. *Cell Mol Life Sci* **66**(20): 3241-3261.
- Andrews NC (1999) Disorders of iron metabolism. *N Engl J Med* **341**(26): 1986-1995.
- Beedle AM, Hamid J and Zamponi GW (2002) Inhibition of transiently expressed low- and high-voltage-activated calcium channels by trivalent metal cations. *J MembrBiol* **187**(3): 225-238.
- Bradbury MW (1997) Transport of iron in the blood-brain-cerebrospinal fluid system. *J Neurochem* **69**(2): 443-454.
- Chattipakorn N, Kumfu S, Fucharoen S and Chattipakorn S (2011) Calcium channels and iron uptake into the heart. *World J Cardiol* **3**(7): 215-218.
- Clark P, Britton LJ and Powell LW (2010) The diagnosis and management of hereditary haemochromatosis. *Clin Biochem Rev* **31**(1): 3-8.
- Donovan A, Brownlie A, Zhou Y, Shepard J, Pratt SJ, Moynihan J, Paw BH, Drejer A, Barut B, Zapata A, Law TC, Brugnara C, Lux SE, Pinkus GS, Pinkus JL, Kingsley PD, Palis J, Fleming MD, Andrews NC and Zon LI (2000) Positional cloning of zebrafish ferroportin1 identifies a conserved vertebrate iron exporter. *Nature* **403**(6771): 776-781.

MOL #80184

Dorey C, Cooper C, Dickson DP, Gibson JF, Simpson RJ and Peters TJ (1993) Iron speciation at physiological pH in media containing ascorbate and oxygen. *Br J Nutr* **70**(1): 157-169.

Elinder F and Arhem P (2003) Metal ion effects on ion channel gating. *Q Rev Biophys* **36**(4): 373-427.

Gaasch JA, Geldenhuys WJ, Lockman PR, Allen DD and Van der Schyf CJ (2007) Voltage-gated calcium channels provide an alternate route for iron uptake in neuronal cell cultures. *Neurochem Res* **32**: 1686-1693.

Ganz T (2011) Heparin and iron regulation, 10 years later. *Blood* **117**(17): 4425-4433.

Garrick MD, Kuo HC, Vargas F, Singleton S, Zhao L, Smith JJ, Paradkar P, Roth JA and Garrick LM (2006) Comparison of mammalian cell lines expressing distinct isoforms of divalent metal transporter 1 in a tetracycline-regulated fashion. *Biochem J* **398**(3): 539-546.

Giorgio M, Trinei M, Migliaccio E and Pelicci PG (2007) Hydrogen peroxide: a metabolic by-product or a common mediator of ageing signals? *Nat Rev Mol Cell Biol* **8**(9): 722-728.

Hering J, Feltz A and Lambert RC (2004) Slow inactivation of the Ca<sub>v</sub>3.1 isotype of T-type calcium channels. *J Physiol (Lond)* **555**: 331-334.

Hess P and Tsien RW (1984) Mechanism of ion permeation through calcium channels. *Nature* **309**(5967): 453-456.

Hodgkin AL and Huxley AF (1952) The components of membrane conductance in the giant axon of *Loligo*. *J Physiol (Lond)* **116**: 473-496.

MOL #80184

Horwitz LD and Rosenthal EA (1999) Iron-mediated cardiovascular injury. *Vasc Med* **4**(2): 93-99.

Huang L, Keyser BM, Tagmose TM, Hansen JB, Taylor JT, Zhuang H, Zhang M, Ragsdale DS and Li M (2004) NNC 55-0396 [(1S,2S)-2-(2-(N-[(3-benzimidazol-2-yl)propyl]-N-methylamino)ethyl)-6-fluoro-1,2,3,4-tetrahydro-1-isopropyl-2-naphthyl cyclopropanecarboxylate dihydrochloride]: A new selective inhibitor of T-type calcium channels *J Pharmacol Exp Ther* **309**: 193-199.

Iancu TC, Shiloh H, Link G, Bauminger ER, Pinson A and Hershko C (1987) Ultrastructural pathology of iron-loaded rat myocardial cells in culture. *Br J Exp Pathol* **68**(1): 53-65.

Kang HW, Park JY, Jeong SW, Kim JA, Moon HJ, Perez-Reyes E and Lee JH (2005) A molecular determinant of nickel inhibition in Cav3.2 T-type calcium channels. *J Biol Chem* **281**: 4823-4830.

Khan N, Gray IP, Obejero-Paz CA and Jones SW (2008) Permeation and gating in Cav3.1 ( $\alpha 1G$ ) T-type calcium channels. Effects of  $Ca^{2+}$ ,  $Ba^{2+}$ ,  $Mg^{2+}$ , and  $Na^{+}$ . *J Gen Physiol* **132**(2): 223-238.

Kim E, Giri SN and Pessah IN (1995) Iron(Ii) Is a Modulator of Ryanodine-Sensitive Calcium Channels of Cardiac-Muscle Sarcoplasmic-Reticulum. *Toxicol Appl Pharm* **130**(1): 57-66.

Kremastinos DT and Farmakis D (2011) Iron overload cardiomyopathy in clinical practice. *Circulation* **124**: 2253-2263.

MOL #80184

Kumfu S, Chattipakorn S, Chinda K, Fucharoen S and Chattipakorn N (2012) T-type calcium channel blockade improves survival and cardiovascular function in thalassemic mice. *Eur J Haematol* **88**(6): 535-548.

Kumfu S, Chattipakorn S, Srichairatanakool S, Settakorn J, Fucharoen S and Chattipakorn N (2011) T-type calcium channel as a portal of iron uptake into cardiomyocytes of beta-thalassemic mice. *Eur J Haematol* **86**(2): 156-166.

Kuryshv YA, Brittenham GM, Fujioka H, Kannan P, Shieh CC, Cohen SA and Brown AM (1999) Decreased sodium and increased transient outward potassium currents in iron-loaded cardiac myocytes. Implications for the arrhythmogenesis of human siderotic heart disease. *Circulation* **100**(6): 675-683.

Kwiatkowski JL (2011) Management of transfusional iron overload - differential properties and efficacy of iron chelating agents. *J Blood Med* **2**: 135-149.

Lane DJ, Robinson SR, Czerwinska H, Bishop GM and Lawen A (2010) Two routes of iron accumulation in astrocytes: ascorbate-dependent ferrous iron uptake via the divalent metal transporter (DMT1) plus an independent route for ferric iron. *Biochem J* **432**(1): 123-132.

Liuzzi JP, Aydemir F, Nam H, Knutson MD and Cousins RJ (2006) Zip14 (Slc39a14) mediates non-transferrin-bound iron uptake into cells. *Proc Natl Acad Sci U S A* **103**(37): 13612-13617.

Lopin KV, Obejero-Paz CA and Jones SW (2010) Evaluation of a two-site, three-barrier model for permeation in Ca<sub>v</sub>3.1 ( $\alpha$ 1G) T-type calcium channels: Ca<sup>2+</sup>, Ba<sup>2+</sup>, Mg<sup>2+</sup>, and Na<sup>+</sup>. *J Membr Biol* **235**(2): 131-143.

MOL #80184

- Lopin KV, Thévenod F, Page JC and Jones SW (2012) Cd<sup>2+</sup> block and permeation in Ca<sub>v</sub>3.1 (α1G) T-type calcium channels. A candidate mechanism for Cd<sup>2+</sup> influx. *Molecular Pharmacology*, submitted.
- Loreal O, Gosriwatana I, Guyader D, Porter J, Brissot P and Hider RC (2000) Determination of non-transferrin-bound iron in genetic hemochromatosis using a new HPLC-based method. *J Hepatol* **32**(5): 727-733.
- Mills E, Dong XP, Wang F and Xu H (2010) Mechanisms of brain iron transport: insight into neurodegeneration and CNS disorders. *Future Med Chem* **2**(1): 51-64.
- Mwanjewe J and Grover AK (2004) Role of transient receptor potential canonical 6 (TRPC6) in non-transferrin-bound iron uptake in neuronal phenotype PC12 cells. *Biochem J* **378**(Pt 3): 975-982.
- Nemeth E, Tuttle MS, Powelson J, Vaughn MB, Donovan A, Ward DM, Ganz T and Kaplan J (2004) Heparin regulates cellular iron efflux by binding to ferroportin and inducing its internalization. *Science* **306**(5704): 2090-2093.
- Obejero-Paz CA, Gray IP and Jones SW (2008) Ni<sup>2+</sup> block of Ca<sub>v</sub>3.1 (α1G) T-type calcium channels. *J Gen Physiol* **132**(2): 239-250.
- Oshiro S, Morioka MS and Kikuchi M (2011) Dysregulation of iron metabolism in Alzheimer's disease, Parkinson's disease, and amyotrophic lateral sclerosis. *Adv Pharmacol Sci* **2011**: 378278.
- Oudit GY, Sun H, Trivieri MG, Koch SE, Dawood F, Ackerley C, Yazdanpanah M, Wilson GJ, Schwartz A, Liu PP and Backx PH (2003) L-type Ca<sup>2+</sup> channels provide a major pathway for iron entry into cardiomyocytes in iron-overload cardiomyopathy. *Nat Med* **9**(9): 1187-1194.

MOL #80184

- Park CH, Valore EV, Waring AJ and Ganz T (2001) Heparin, a urinary antimicrobial peptide synthesized in the liver. *J Biol Chem* **276**(11): 7806-7810.
- Parkes JG, Liu Y, Sirna JB and Templeton DM (2000) Changes in gene expression with iron loading and chelation in cardiac myocytes and non-myocytic fibroblasts. *J Mol Cell Cardiol* **32**(2): 233-246.
- Pelizzoni I, Macco R, Morini MF, Zacchetti D, Grohovaz F and Codazzi F (2011) Iron handling in hippocampal neurons: activity-dependent iron entry and mitochondria-mediated neurotoxicity. *Aging Cell* **10**(1): 172-183.
- Perez-Reyes E (2003) Molecular physiology of low-voltage-activated T-type calcium channels. *Physiol Rev* **83**(1): 117-161.
- Rodman DM, Reese K, Harral J, Fouty B, Wu S, West J, Hoedt-Miller M, Tada Y, Li KX, Cool C, Fagan K and Cribbs L (2005) Low-voltage-activated (T-type) calcium channels control proliferation of human pulmonary artery myocytes. *Circ Res* **96**: 864-872.
- Serrano JR, Dashti SR, Perez-Reyes E and Jones SW (2000) Mg<sup>2+</sup> block unmasks Ca<sup>2+</sup>/Ba<sup>2+</sup> selectivity of  $\alpha$ 1G T-type calcium channels. *Biophys J* **79**(6): 3052-3062.
- Serrano JR, Perez-Reyes E and Jones SW (1999) State-dependent inactivation of the  $\alpha$ 1G T-type calcium channel. *J Gen Physiol* **114**(2): 185-201.
- Stankiewicz JM and Brass SD (2009) Role of iron in neurotoxicity: a cause for concern in the elderly? *Curr Opin Clin Nutr Metab Care* **12**(1): 22-29.

MOL #80184

- Traboulsie A, Chemin J, Chevalier M, Quignard JF, Nargeot J and Lory P (2007)  
Subunit-specific modulation of T-type calcium channels by zinc. *J Physiol* **578**(Pt 1): 159-171.
- Tsushima RG, Wickenden AD, Bouchard RA, Oudit GY, Liu PP and Backx PH (1999)  
Modulation of iron uptake in heart by L-type Ca<sup>2+</sup> channel modifiers: possible implications in iron overload. *Circ Res* **84**(11): 1302-1309.
- Viollier E, Inglett PW, Hunter K, Roychoudhury AN and Van Cappellen P (2000) The ferrozine method revisited: Fe(II)/Fe(III) determination in natural waters. *Appl Geochem* **15**(6): 785-790.
- Wan S, Hua Y, Keep RF, Hoff JT and Xi G (2006) Deferoxamine reduces CSF free iron levels following intracerebral hemorrhage. *Acta Neurochir Suppl* **96**: 199-202.
- Wang SM, Fu LJ, Duan XL, Crooks DR, Yu P, Qian ZM, Di XJ, Li J, Rouault TA and Chang YZ (2010) Role of hepcidin in murine brain iron metabolism. *Cell Mol Life Sci* **67**(1): 123-133.
- Winegar BD, Kelly R and Lansman JB (1991) Block of current through single calcium channels by Fe, Co, and Ni. Location of the transition metal binding site in the pore. *J Gen Physiol* **97**(2): 351-367.
- Woodhull AM (1973) Ionic blockage of sodium channels in nerve. *J Gen Physiol* **61**: 687-708.
- Yunker AMR and McEnery MW (2003) Low voltage-activated ("T-type") calcium channels in review. *J Bioenerg Biomembr* **35**: 533-575.
- Zhang AS and Enns CA (2009) Molecular mechanisms of normal iron homeostasis. *Hematology Am Soc Hematol Educ Program*: 207-214.

MOL #80184

Zhou W and Jones SW (1995) Surface charge and calcium channel saturation in bullfrog sympathetic neurons. *J Gen Physiol* **105**(4): 441-462.

MOL #80184

## Footnotes

This study was supported by the National Institutes of Health, National Institute of Neurological Diseases and Stroke [NS24471], and FT Deutsche Forschungsgemeinschaft [TH345/11-1] and Stiftung Westermann-Westdorp.

Correspondence to Stephen W. Jones, Department of Physiology and Biophysics, Case Western Reserve University, Cleveland, OH 44106.

Current affiliation of Carlos A. Obejero-Paz: ChanTest Corporation, Cleveland, OH 44128.

MOL #80184

## Figure Legends

**Fig. 1.** Block by  $\text{Fe}^{2+}$  of currents carried by  $\text{Ca}^{2+}$  with the IIV protocol. A, sample records of currents, using the protocol illustrated below the middle record, in control (left), after addition of  $\text{Fe}^{2+}$  (middle), and after washout of  $\text{Fe}^{2+}$  (right). 3 kHz Gaussian filter. Currents shown here are in 40 mV increments. B, IIV relations from the protocol of A, in control (0  $\text{Fe}^{2+}$ ), and in two concentrations of  $\text{Fe}^{2+}$  ( $n=4$  for each concentration). C, expanded view of IIV relations. D, chord conductances calculated for the data from B. E, Inhibition by  $\text{Fe}^{2+}$ , expressed as the ratio of the chord conductance in  $\text{Fe}^{2+}$  to the chord conductance in control conditions. Data not shown near the reversal potential, where errors in calculating conductances can be large. Solid curves are fits to a Woodhull (1973) model. Symbols in B apply to panels B-E.

**Fig. 2.** Block by  $\text{Fe}^{2+}$  of currents carried by  $\text{Ca}^{2+}$  using the IV protocol. A, sample records, shown in 20 mV increments, with 3 kHz Gaussian filter. B, IV relations from the protocol of A, for the same cells as Fig. 1. C, IV relations on an expanded scale. D, chord conductances from the data of B. E, inhibition by  $\text{Fe}^{2+}$ , as the chord conductance ratio, fitted to a Woodhull (1973) model. Data not shown near the reversal potential. Symbols in B apply to panels B-E.

**Fig. 3.** Effects of  $\text{Fe}^{2+}$  on gating. A, effect of  $\text{Fe}^{2+}$  on the time-to-peak of currents, using the IV protocol. B, effect of  $\text{Fe}^{2+}$  on the time constant for deactivation, using the IIV protocol. C, effect of  $\text{Fe}^{2+}$  on channel activation, as the ratio of the peak IV current to the IIV current at the same voltage. D, voltage shifts for the data shown in A-C, for the activation curve ( $\Delta P_{O,r}$ ), for deactivation ( $\Delta \tau_{\text{IIV}}$ ), and for time to peak ( $\Delta t_{\text{Peak}}$ ). The solid curve is a fit to Gouy-Chapman-Stern theory. The dashed curve is the fit to voltage shifts

MOL #80184

induced by  $\text{Ca}^{2+}$ ,  $\text{Ba}^{2+}$ , and  $\text{Mg}^{2+}$ , from Khan et al. (2008). Symbols in A apply to panels A-C. Data not shown near the reversal potential in A-C. Same cells as Figs. 1-2.

**Fig. 4.** Effects of  $\text{Fe}^{2+}$  with 2 mM  $\text{Ba}^{2+}$  as charge carrier. A, sample records with the IIV protocol, 40 mV increments. B, sample records with the IV protocol, 20 mV increments. 3 kHz Gaussian filter.

**Fig. 5.** Analysis of effects of  $\text{Fe}^{2+}$  in 2 mM  $\text{Ba}^{2+}$ . A, IIV relations in control and in 0.13 mM  $\text{Fe}^{2+}$ . B, inhibition by  $\text{Fe}^{2+}$ , from the ratio of chord conductances ( $\text{Fe}^{2+}/\text{control}$ ), fitted to a Woodhull (1973) model. C, IV relations (currents from +50 to +100 mV not shown). D, activation curves, from IV/IIV current ratios. Data not shown near the reversal potential in B and D.  $n=4$  for all panels.

**Fig. 6.** Permeation by  $\text{Fe}^{2+}$ . A, sample records with the IIV protocol, in 40 mV increments, with 3 kHz Gaussian filter. The inset below the middle record shows currents from -100 to +20 mV, on a 5-fold expanded scale. B, IIV relations. C, IIV relations on an expanded scale. Symbols in C also apply to B. Data in B-C are from 7 cells, 4 in 1.1 mM  $\text{Fe}^{2+}$ , 5 in 8.9 mM  $\text{Fe}^{2+}$ .

**Fig. 7.** Comparison of tail currents in  $\text{Fe}^{2+}$  to gating currents. A, sample records with the IIV protocol, in 40 mV increments. Note partial recovery (right panel) following superfusion with the solution used to isolate gating currents ( $\text{La}^{3+} + \text{Cd}^{2+}$ ). The insets below the middle two records are on a  $5\times$  expanded scale, to show tail currents in  $\text{Fe}^{2+}$  and on- and off gating currents in  $\text{La}^{3+} + \text{Cd}^{2+}$ . 3 kHz Gaussian filter. B, integrated tail currents in  $\text{Fe}^{2+}$  compared to  $Q_{\text{on}}$  (measured during depolarization to +60 mV) and  $Q_{\text{off}}$  (measured following repolarization).  $n=5$  ( $\text{Fe}^{2+}$  tails) and  $n=4$  ( $Q_{\text{on}}$  and  $Q_{\text{off}}$ ). C, the portion of the integrated tail current amplitude attributable to  $\text{Fe}^{2+}$  entry, as a function of

MOL #80184

$\text{Fe}^{2+}$ , for the 5 cells in B, and 2 cells tested at  $\sim 1 \text{ mM Fe}^{2+}$ . The solid curve is a fit to a single saturable binding site with  $K_D = 4.7 \text{ mM}$  and maximal  $Q = 0.78 \text{ pC}$ .

**Fig. 8.** A 2S3B Eyring model for permeation and block by  $\text{Fe}^{2+}$ . A, energy levels and electrical distances for barriers and wells, for  $\text{Ca}^{2+}$  and  $\text{Fe}^{2+}$ . Energy levels (outside to inside) were 9.32, -12.73, 5.26, -6.97, and 15.65 RT. The electrical distances and energy profiles for  $\text{Na}^+$ ,  $\text{Mg}^{2+}$ , and  $\text{Ba}^{2+}$  are from Lopin et al. (2011). B to D, fits of the model to experimental IIV data are shown for permeation (B), block of current carried by 2 mM  $\text{Ca}^{2+}$  (C), and block with 2 mM  $\text{Ba}^{2+}$  (C). E, calculation of the rate of  $\text{Fe}^{2+}$  entry for the indicated  $\text{Fe}^{2+}_o$  concentrations, in the presence of 2 mM  $\text{Ca}^{2+}_o$ , for a single open channel. F, calculation of the steady-state rate of  $\text{Fe}^{2+}$  entry considering channel gating (activation and inactivation). The steady-state  $P_O$ -V relationship calculated from the Serrano et al. (1999) model was convolved with the curves in panel E.

Figure 1

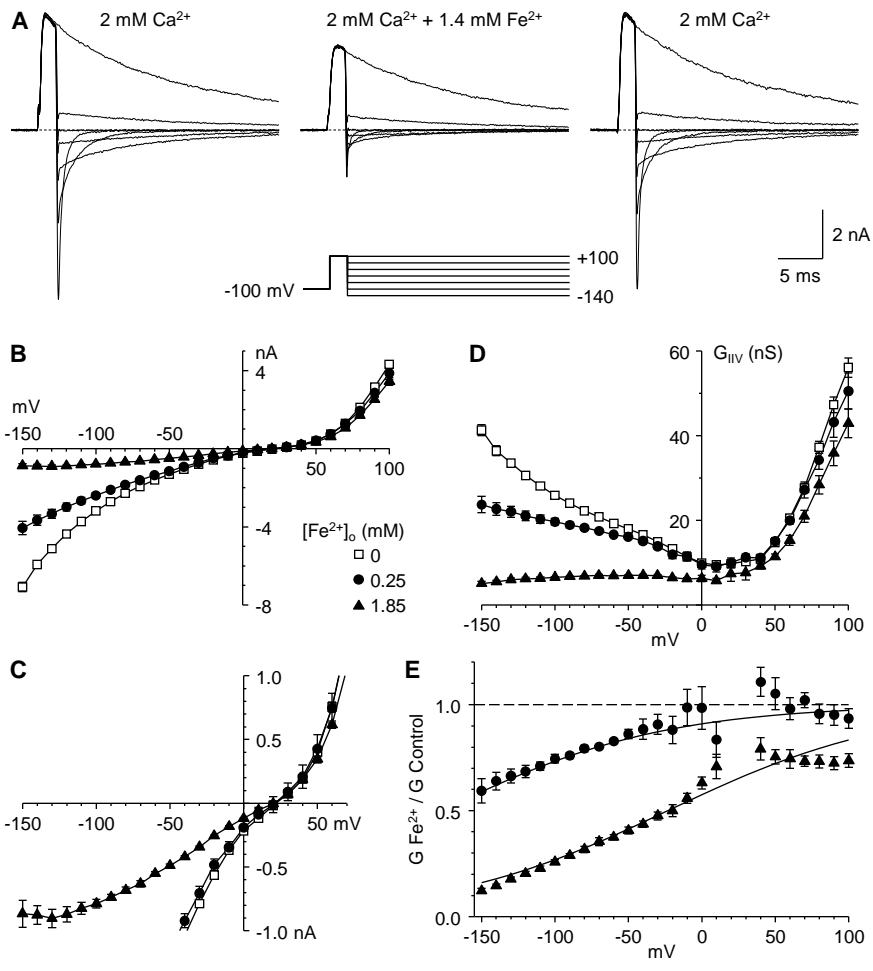


Figure 2

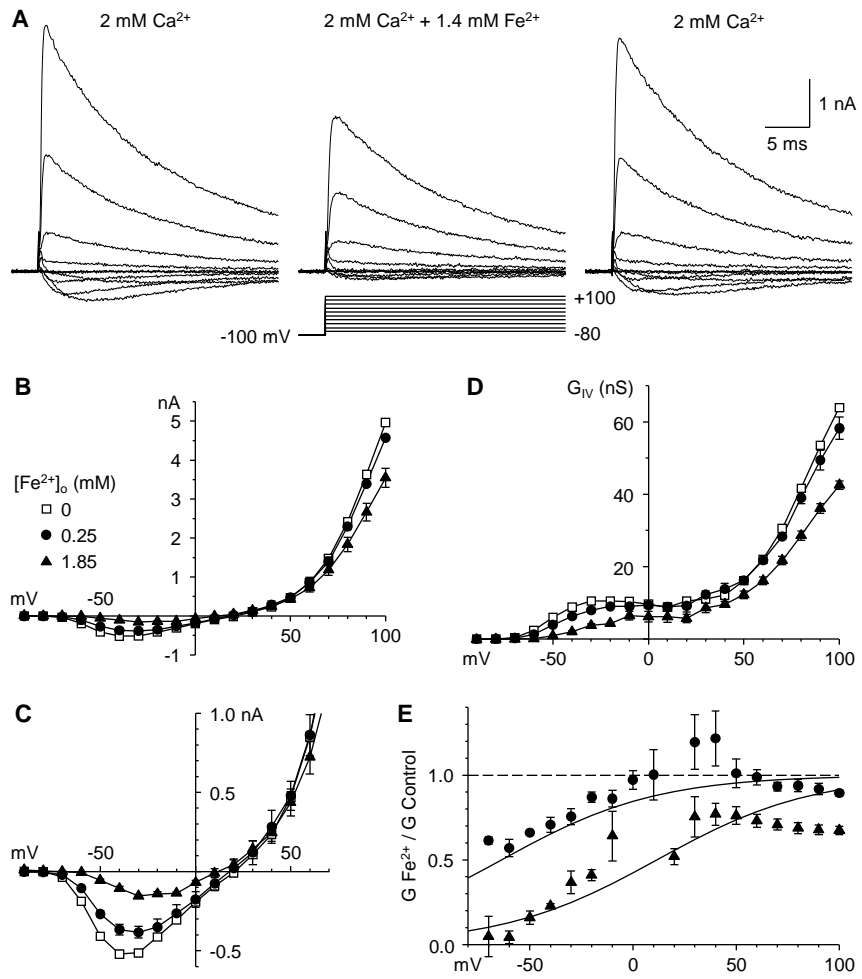


Figure 3

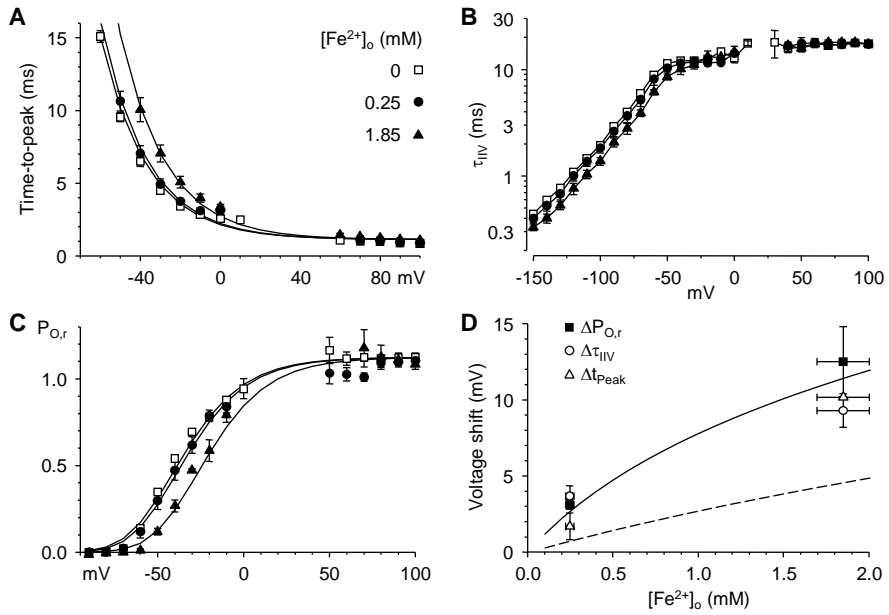


Figure 4

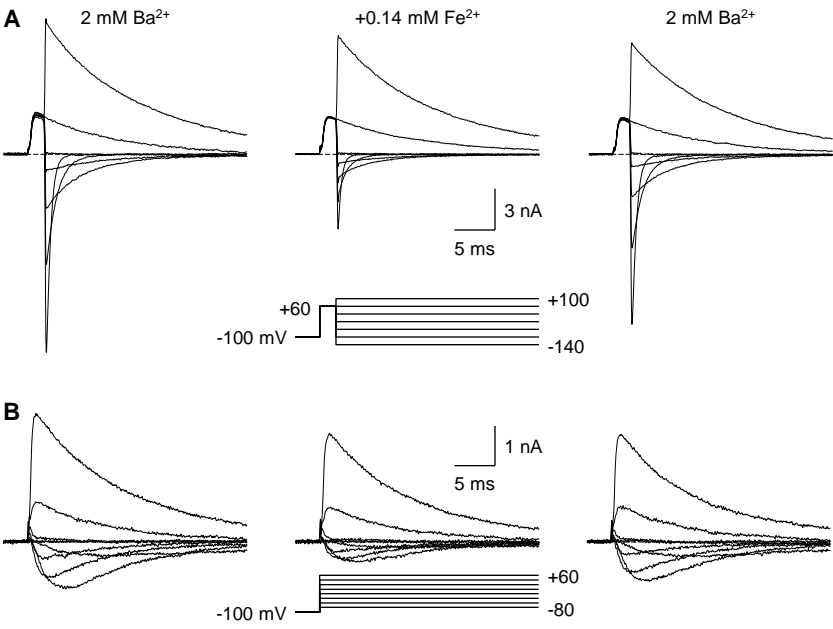


Figure 5

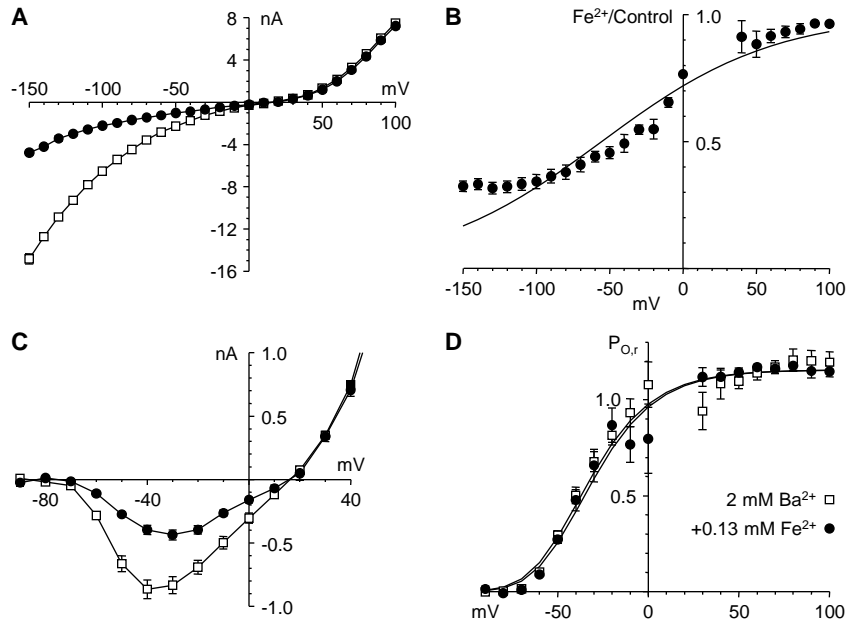


Figure 6

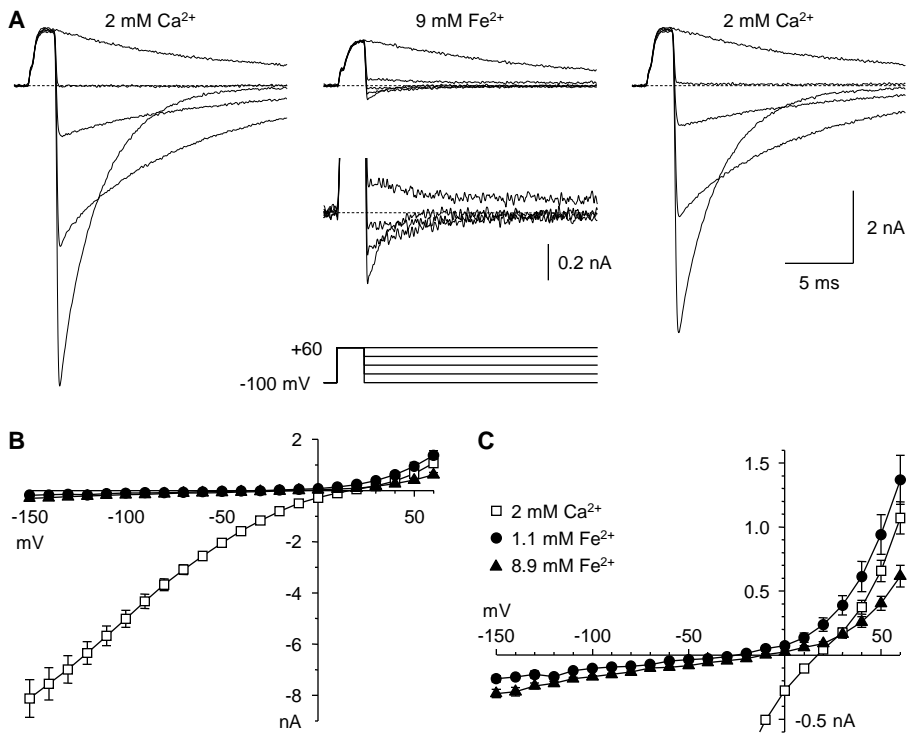


Figure 7

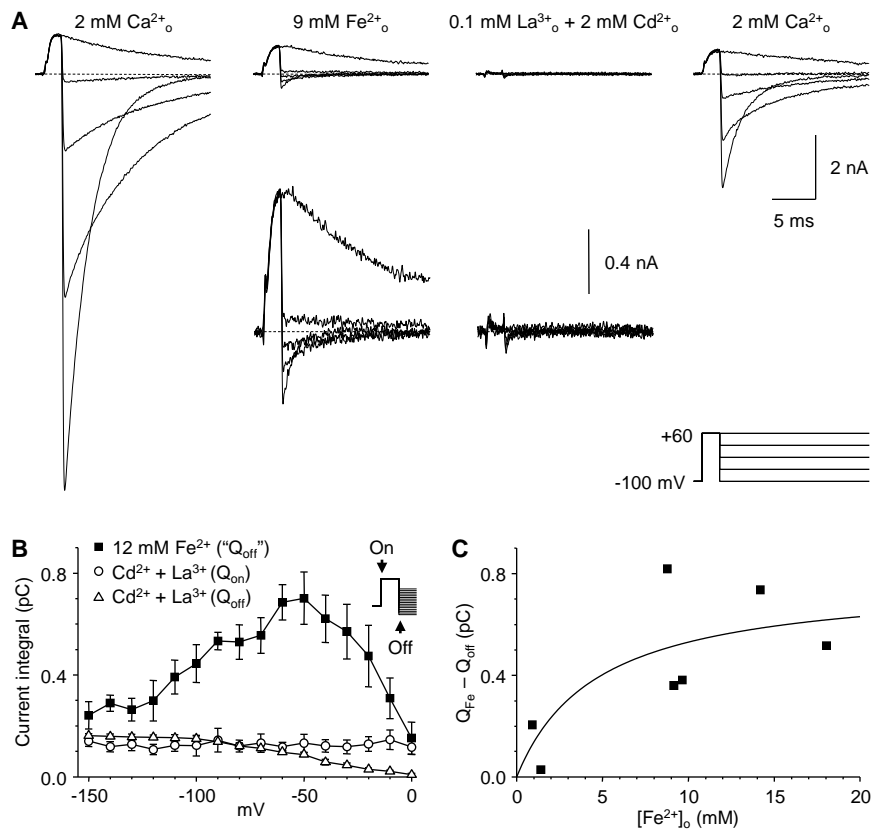


Figure 8

